PCP
PLANT & CELL PHYSIOLOGY

Lipidomic Analysis of Arabidopsis T-DNA Insertion Lines Leads to Identification and Characterization of C-Terminal Alterations in FATTY ACID DESATURASE 6

Hannah J. Lusk[1,4,†], Nicholas Neumann[1,†], Madeline Colter[2], Mary R. Roth[2], Pamela Tamura[2], Libin Yao[2], Sunitha Shiva[2,5], Jyoti Shah[3], Kathrin Schrick[2], Timothy P. Durrett[1,*] and Ruth Welti[2,*]

[1]Department of Biochemistry and Molecular Biophysics, Kansas State University, 1711 Claflin Rd., Manhattan, KS 66506, USA
[2]Division of Biology, Kansas State University, 1717 Claflin Rd., Manhattan, KS 66506, USA
[3]Department of Biological Sciences and BioDiscovery Institute, University of North Texas, 1155 Union Circle #305220, Denton, TX 76203-5017, USA
[4]Present address: Department of Chemistry and Biochemistry, University of California, Santa Cruz, Division of Physical & Biological Sciences, 1156 High Street, Santa Cruz, CA 95064, USA
[5]Present address: Eurofins Scientific, 4780 Discovery Drive, Columbia, MO 65201, USA
[†]These authors contributed equally.

*Corresponding authors: Timothy Durrett, E-mail, tdurrett@ksu.edu; Ruth Welti, E-mail, welti@ksu.edu

(Received 18 April 2022; Accepted 20 June 2022)

Regular Paper

Mass-spectrometry-based screening of lipid extracts of wounded and unwounded leaves from a collection of 364 *Arabidopsis thaliana* T-DNA insertion lines produced lipid profiles that were scored on the number and significance of their differences from the leaf lipid profiles of wild-type plants. The analysis identified Salk_109175C, which displayed alterations in leaf chloroplast glycerolipid composition, including a decreased ratio between two monogalactosyldiacylglycerol (MGDG) molecular species, MGDG(18:3/16:3) and MGDG(18:3/18:3). Salk_109175C has a confirmed insertion in the *At5g64790* locus; the insertion did not co-segregate with the recessive lipid phenotype in the F2 generation of a wild-type (Columbia-0) × Salk_109175C cross. The altered lipid compositional phenotype mapped to the *At4g30950* locus, which encodes the plastidial ω-6 desaturase FATTY ACID DESATURASE 6 (FAD6). Sequencing revealed a splice-site mutation, leading to the in-frame deletion of 13 amino acids near the C-terminal end of the 448 amino acid protein. Heterologous expression in yeast showed that this deletion eliminates desaturase activity and reduces protein stability. Sequence comparison across species revealed that several amino acids within the deletion are conserved in plants and cyanobacteria. Individual point mutations in four conserved residues resulted in 77–97% reductions in desaturase activity, while a construct with all four alanine substitutions lacked activity. The data suggest that the deleted region of *FAD6*, which is on the C-terminal side of the four putative transmembrane segments and the histidine boxes putatively involved in catalysis, is critical for FAD6 function.

Keywords: *Arabidopsis thaliana* ● Fatty acid desaturase ● Lipidomics ● Mass spectrometry

Introduction

FATTY ACID DESATURASE 6, or FAD6, is an ω-6 fatty acid desaturase that catalyzes the introduction of a double bond in the biosynthesis of 16:3 and 18:3 fatty acids using soluble ferredoxin as an electron donor (Browse et al. 1989, Schmidt and Heinz 1993, Falcone et al. 1994). It is a 448-residue (∼48 kDa) integral membrane protein that resides in the chloroplast inner membrane (Schmidt and Heinz 1990, Falcone et al. 1994). FAD6 catalyzes the biosynthetic conversions of *cis*-7-16:1 to *cis*,*cis*-7,10-16:2 and *cis*-9-18:1 to *cis*,*cis*-9,12-18:2, which are subsequently converted to the trienoic fatty acids (all *cis*-7,10,13-16:3 and all *cis*-9,12,15-18:3). The desaturase reactions occur in fatty acids esterified to the galactoglycerolipids, monogalactosyldiacylglycerol (MGDG) and digalactosyldiacylglycerol (DGDG), phosphatidylglycerol (PG) and sulfoquinovosyldiacylglycerol (SQDG). The sequence analysis of FAD6 revealed the presence of three histidine-rich motifs (histidine boxes) that are believed to be involved in the formation of catalytically active complexes that bind iron (Falcone et al. 1994, Schmidt et al. 1994). Despite access to sequence information, structural and functional analyses of this desaturase are needed to fully understand its molecular function. Our understanding of membrane-bound desaturases, in general, has lagged behind that of soluble desaturases, largely due to technical challenges in structural analysis and direct functional investigation.

Plant Cell Physiol. 63(9): 1193–1204 (2022) doi:https://doi.org/10.1093/pcp/pcac088, Advance Access publication on 21 June 2022, available online at https://academic.oup.com/pcp

Besides its role in chloroplast membrane biogenesis, FAD6 is involved in plant adaptation to stress conditions, including cold stress and salt stress (Hugly and Somerville 1992, Carlsson et al. 2002, Zhang et al. 2009). *FAD6* mutants display a chlorotic phenotype during cold stress, with alterations in chloroplast organization and ultrastructure in newly developed leaves (Hugly and Somerville 1992). Mutations in *FAD6* have been shown to suppress and rescue phenotypes of other Arabidopsis mutants. For example, despite the poor performance of *fad6* mutants in the cold, a *fad6* mutation reduces the severity of the chilling-sensitive phenotype of the *fatty acid biosynthesis 1* (*fab1*) mutant (Gao et al. 2015). Mutant alleles of *FAD6* also suppress the small-size phenotype of *fatty acid biosynthesis 2* (*fab2*; also known as *ssi2*) (Kachroo et al. 2003, Nandi et al. 2003) and *fab2*'s cell-death-related phenotypes (Nandi et al. 2003), although the underlying mechanisms have not been fully elucidated.

In this study, we identified a new allelic mutant of *FAD6* (*fad6-3*) from the analysis of Arabidopsis transfer-DNA (T-DNA) insertion line Salk_109175C. The mutation results in decreased levels of MGDG(18:3/16:3) in leaves. Molecular characterization revealed that the mutation causes an in-frame deletion of 13 amino acids in the FAD6 protein, leading to a complete loss of desaturase activity in a yeast expression system. Analysis of the deleted sequence revealed that multiple amino acids in this region are conserved in other plants and cyanobacteria. Additional *fad6* mutants were generated and their catalytic activity was tested in yeast to determine the role of the phylogenetically conserved residues affected by the *fad6-3* mutation.

Results

Lipidomic analysis identified Salk insertional mutants with altered lipid compositions

A group of confirmed Salk T-DNA insertion lines (Alonso et al. 2003) was obtained from Arabidopsis Biological Resource Center (ABRC, Ohio State, Columbus, OH, USA) and used, without further genetic analysis, to screen for differences in lipid composition, in comparison to wild-type plants. The Salk lines putatively contained insertions in 364 genes (**Supplementary Table S1**), most of which are involved or putatively involved in lipid metabolism. The leaf lipids from an unwounded and a wounded leaf from three plants of each insertion line were analyzed using direct-infusion electrospray ionization triple quadrupole mass spectrometry (Vu et al. 2014). The data are presented both as normalized intensity per milligram of leaf dry mass, where a signal of 1 corresponds to the same amount of signal as derived from 1 pmol of internal standard(s), and as a percent of the total normalized intensity for analyzed lipids (**Supplementary Tables S2–S5**). The decision to include wounded and unwounded plants in the analysis was motivated by the desire to capture stress-induced lipids as well as those present under basal conditions. The data for each line were compared to those of wild-type plants grown on the same trays using *t*-tests, and *P* values were calculated (**Supplementary Tables S6–S9**). The *P* values were used to calculate scores for the overall difference between the lipids of each line and those of wild-type plants for both unwounded and wounded plants (**Supplementary Table S10**). The lines with the largest differences in leaf lipid amounts and/or percentages as compared to wild-type plants are shown in **Table 1**. The Salk_109175C line exhibited the largest difference in leaf lipids, as compared to wild-type plants.

Table 1 Salk T-DNA insertion line with measured leaf lipids differing the most from wild type in lipid levels and/or composition, from 364 lines analyzed under control conditions and after wounding.

Name of line	Associated gene	Gene description
Salk_109175C	*At5g64790*	More information on this Salk line is included in this paper
Salk_134251C	*At1g02660*	PLIP2; PLASTID LIPASE2
Salk_137481C	*At5g53390*	WSD11; wax ester synthase/DGAT family protein
Salk_065859C	*At4g39960*	Hsp40; molecular chaperone
Salk_049668C	*At1g58520*	RXW8; GDSL-like lipase/acylhydrolase superfamily protein
Salk_030535C	*At5g16120*	MAGL15; alpha/beta-hydrolase superfamily protein
Salk_111635C	*At1g28640*	GDSL-motif esterase/acyltransferase/lipase
Salk_065071C	*At1g28600*	GDSL-motif esterase/acyltransferase/lipase
Salk_062226C	*At4g18970*	GDSL-motif esterase/acyltransferase/lipase
Salk_076158C	*At5g41900*	BDG2; alpha/beta-hydrolase superfamily protein
Salk_029716C	*At1g78690*	Lysoglycerophospholipid *O*-acyltransferase
Salk_047440C	*At1g67560*	LOX6; LIPOXYGENASE 6
Salk_136051C	*At2g45670*	LPEAT2, LYSOPHOSPHATIDYLETHANOLAMINE ACYLTRANSFERASE2
Salk_067533C	*At3g15730*	PLDα1; PHOSPHOLIPASE Dα1
Salk_141343C	*At5g60620*	GPAT9; GLYCEROL-3-PHOSPHATE ACYLTRANSFERASE9
Salk_052637C	*At2g38180*	SGNH hydrolase-type esterase superfamily protein
Salk_113245C	*At2g19010*	GDSL-motif esterase/acyltransferase/lipase
Salk_105449C	*At5g55050*	GDSL-motif esterase/acyltransferase/lipase
Salk_024839C	*At4g37050*	PLP4; PATATIN-LIKE PROTEIN4 [also known as pPLA-IIγ (Scherer et al. 2010)]
Salk_123787C	*At4g34920*	PLC-like phosphodiesterase superfamily protein

Salk_109175C has low levels of chloroplast-assembled membrane glycerolipids

The T-DNA insertion line Salk_109175C has a confirmed mutation in *At5g64790*, a poorly characterized gene annotated as encoding an *O*-glycosyl hydrolase. Repeating the leaf lipid analysis on a large number (18) of replicate plants of Salk_109175C revealed differences across the lipidome (**Supplementary Table S11**). In particular, significant

differences in several MGDG species, as well as other alterations in chloroplast glycerolipid composition, were observed (**Fig. 1A** and **Supplementary Fig. S1**). Among the differences in Salk_109175C, compared to wild-type plants, was a much lower level of chloroplast-assembled MGDG(18:3/16:3), also called MGDG(34:6) (**Fig. 1A**). The ratio of 34:6 to 36:6 molecular species in the MGDG and DGDG classes was lower in leaves of Salk_109175C than in leaves of wild-type plants, suggesting that the level of fatty acid 16:3 was lower in Salk_109175 than in wild type.

Comprehensive profiling of wild-type and Salk_109175C untreated and wounded plants indicated that several other chloroplast-assembled, 34-carbon and polyunsaturated glycerolipid species were lower in leaves of Salk_109175C compared to leaves of wild-type plants (**Supplementary Table S11**). These include SQDG(34:3), MGDG(34:5) and DGDG(34:5) (**Supplementary Fig. S1**). Markedly higher levels of PG(34:2), i.e. primarily PG(18:1/16:1), were observed, with correspondingly lower levels of PG(34:4), i.e. PG(18:3/16:1). The current work also includes glycerolipid profiles of wounded plants (**Supplementary Table S11**). Just as the level of 16:3-containing lipids was lower in leaves of Salk_109175C than in wild-type leaves, 16:3-derived oxidized lipids, such as *dinor*-oxophytodienoic acid (*dn*OPDA), which are produced in response to wounding, were also lower in Salk_109175C. For example, Arabidopside E, which is an oxophytodienoic acid (OPDA) head group-acylated MGDG with OPDA and *dn*OPDA acyl chains on the glycerol, was produced at less than 1% of wild-type levels when the Salk_109175 line was analyzed (**Supplementary Table S11**, lipid0535). In contrast, Arabidopside G, which is a head group-acylated MGDG with three 18-carbon OPDA molecules derived from 18:3, was found at 2.9 times higher levels after wounding the leaves of the Salk_109175 line compared to wild-type leaves (**Supplementary Table S11**, lipid0540).

The mutant lipid phenotype was not linked to the *At5g64790* T-DNA insertional mutation

Salk_109175C has a confirmed mutation (Salk_109175.47.45.x polymorphism) at the *At5g64790* locus, which encodes a putative *O*-glycosyl hydrolase. However, the lipid changes observed in this mutant appeared to be unrelated to glycosyl hydrolase activity. Instead, they resembled lipid changes previously described in mutants of plastid-localized acyltransferases and desaturases. Furthermore, based on eFP Browser analysis (Winter et al. 2007), *At5g64790* is mostly expressed in pollen, whereas the lipid phenotype was observed in leaves, suggesting that the mutation in *At5g64790* was not responsible for the observed lipid phenotype.

To determine whether the phenotype was due to the known insertional mutation in *At5g64790*, the homozygous Salk line was backcrossed with wild-type Columbia-0 (Col-0). The low MGDG(34:6)/MGDG(36:6) phenotype was segregated as a recessive trait in the F2 progeny (**Fig. 1B**). Furthermore, this recessive trait did not co-segregate with the T-DNA insertion at the *At5g64790* locus in Salk_109175. The low

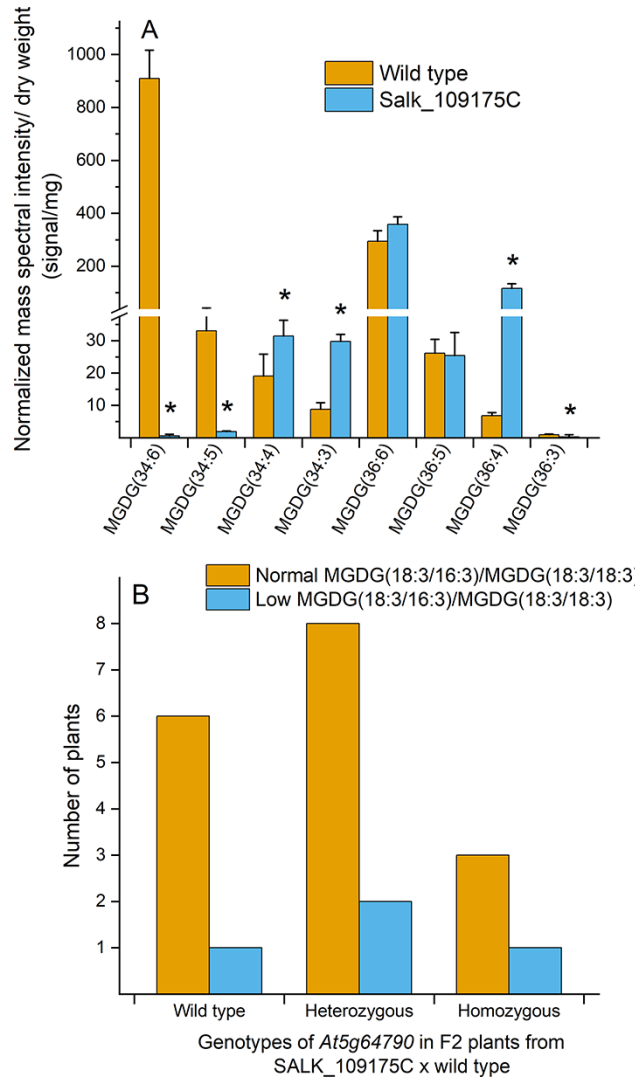

Fig. 1 The lipid phenotype in Salk_109175 is not linked to the At5g64790 T-DNA insertion. (A) Levels of MGDG lipid molecular species in leaves of 30-day-old wild-type (Col-0) and Salk_109175C plants. A signal of 1 corresponds to the same amount of signal as derived from 1 nmol of internal standard(s) with no correction for the relative response of standard lipids compared to analyte lipids. Asterisks indicate a *P* value of <0.01 for comparison of the molecular species between wild type and Salk_109175. The ratio of MGDG(34:6)/MGDG(36:6) was >2 in leaves of wild-type plants (upper panel) and <0.01 in leaves of Salk_109175C plants. (B) Phenotypes of genotyped F2 plants from a cross of wild type (Col-0) and Salk_109175C. Plants were genotyped for the Salk_109175C insertion in *At5g64790* and ratios of plastidic MGDG species. The ratios of MGDG(34:6)/MGDG(36:6) species were determined in the genotyped plants were classified as 'normal', which was a ratio greater than 2, or 'low', a ratio less than 0.1. (No plants with ratios between 0.1 and 2 were observed.) The *Y*-axis indicates the number of plants of each genotype with each phenotype. Data for this figure can be found in **Supplementary Table S11**. In part A, $n = 6$ for wild-type plants and $n = 18$ for Salk_109175C plants.

MGDG(34:6)/MGDG(36:6) phenotype was found in F2 plants that were wild type, heterozygous and homozygous with

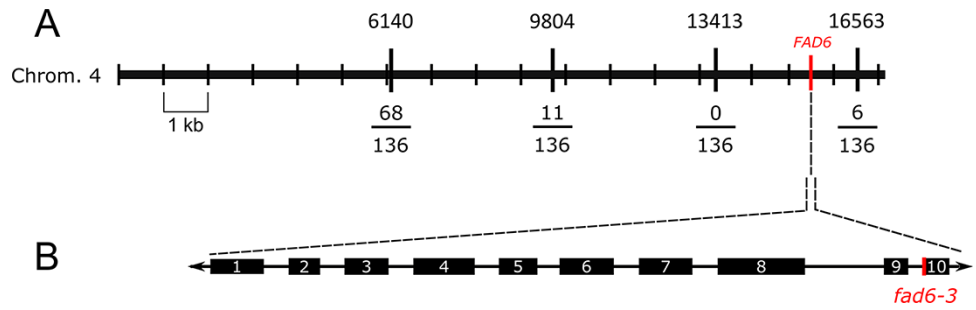

Fig. 2 Mapping of the lipid-related mutation to *FAD6* on chromosome 4. (A) The genotyping of 136 F2 mutant plants mapped the corresponding gene to a 2.1-Mb region between markers 13,413 and 16,563 at the end of chromosome 4. Marker names (above the line representing chromosome 4) correspond to their position (kb) along chromosome 4. The number of recombinant lines for each marker over the total number of F2 mutant lines genotyped is shown below the line. (B) The *FAD6* gene with exons (1–10) is represented by black boxes. The position of the splice-site mutation in *fad6-3* is shown in red.

Table 2 *Arabidopsis thaliana fad6* allelic mutants. Sequences are counted from the start of the coding sequence, i.e. position 1 in TAIR accession sequence 2,126,736 (FAD6 coding sequence) https://www.arabidopsis.org/servlets/TairObject?accession=Sequence:2126736 or position 174 in TAIR accession sequence 4,010,726,749 (FAD6 genomic DNA) at https://www.arabidopsis.org/servlets/TairObject?accession=Sequence:4010726749.

Allele	Coding sequence	Genomic DNA	Amino acid	Reference
sfd4	C398T	C874T	S133F	Nandi et al. (2003)
fad6-1	G478A	G954A	G160R	Browse et al. (1989); Kachroo et al. (2003)
fad6-2	C673T	C1304T	P225S	Xu et al. (2010)
fad6-3	Not in coding sequence	G2231A	Δ13(Y395-K407)	This study

respect to the T-DNA insertion at the *At5g64790* locus (**Fig. 1B**). This lack of co-segregation indicated that the low MGDG(34:6)/MGDG(36:6) phenotype was not linked to the known T-DNA insertion mutation in Salk_109175C.

The reduced level of 16:3 in MGDG in Salk_109175C leaves led us to consider whether the mutation might be in a gene involved in the formation of glycerolipids in the plastid. Like Salk_109175C, a mutant in *ACYLTRANSFERASE1* (*ATS1* or *ACT1*; *At1g32200*) has very low levels of MGDG(34:6) (Falcone et al. 2004; **Supplementary Fig. S2**; **Supplementary Table S12**). To test whether the mutation was in *ATS1*, Salk109175_C was crossed with an *ats1* mutant. The resulting F1 plants produced an average of 76% as much MGDG(34:6) as wild-type plants (**Supplementary Fig. S2**; **Supplementary Table S12**). Thus, the *ats1* mutant was able to complement the recessive low MGDG(34:6) trait in Salk_109175C, indicating that the lipid defect of Salk_109175C is not due to a mutation in *ATS1*.

The altered lipid phenotype mapped to *FAD6*, which encodes a plastid-localized ω6 desaturase

Mapping based on nucleotide polymorphisms between Col-0 and Landsberg *erecta* (L*er*-0) accessions was used to identify the gene associated with the observed lipid compositional changes in Salk_109175C. The mutation associated with the lipid compositional phenotype was mapped to a 2.1-Mb region on chromosome 4 that included the *At4g30950* locus, which encodes the plastid-localized ω-6 fatty acid desaturase *FAD6* (**Fig. 2A**). Sequencing the *FAD6* gene in the mutant showed a single-nucleotide change at the acceptor splice site between exons 9 and 10 (**Fig. 2B**); the corresponding mutant was named *fad6-3*, as the thus far reported *FAD6* loss-of-function alleles are *fad6-1*, *fad6-2* and *sfd4* (**Table 2**; Browse et al. 1989, Kachroo et al. 2003, Nandi et al. 2003, Xu et al. 2010). Complementary DNA (cDNA) sequencing revealed that this G to A transition resulted in the in-frame deletion of nucleotides encoding the first 13 amino acids of exon 10 near the C-terminus of the protein (**Fig. 3**, **Supplementary Fig. S3**). The deletion is downstream of the three histidine boxes and four transmembrane domains, in a region that has not been functionally characterized (**Fig. 3**). The lipid phenotype of *fad6-3* was similar to that of *fad6-1*, suggesting it also represents a loss-of-function mutation (**Fig. 4**). Analysis of the fatty acid composition of leaves from *fad6-1* and *fad6-3* plants shows that 16:2 and 16:3 are absent in both mutants, whereas they both accumulate *cis*-7-16:1 and 18:1 (**Fig. 4A** and **Supplementary Table S13**). Both *fad6-1* and *fad6-3* lack DGDG(34:6), DGDG(34:5) and MGDG(34:6) and exhibit very low levels of MGDG(34:5) and PG(34:4) (**Fig. 4B**). Lipid profiling of other lipid classes is displayed in **Supplementary Fig. S4**, which shows that extraplastidically produced lipids [phosphatidylcholine (PC), phosphatidylethanolamine (PE), phosphatidylinositol, phosphatidylserine, lysoPC and lysoPE (LPE)] are less affected by the mutation than plastidically produced lipids [DGDG, MGDG, PG and lysoPG (LPG)] (**Fig. 4**). Notably, the leaves of the *fad6-1* and *fad6-3* mutants had lower lipid content per dry mass (220 ± 4 and 218 ± 5 nmol mg^{-1}, respectively) compared to wild type (307 ± 13 nmol mg^{-1}), mainly due to a decrease in total MGDG (**Supplementary Table S14**). LPG(18:1) was considerably increased in both *fad6* mutants, whereas LPG(18:3) was decreased (**Supplementary Fig. S4B**). Overall, the data in **Fig. 4** and **Supplementary Fig. S4** demonstrate that the lipid phenotypes of the *fad6-1* and *fad6-3*

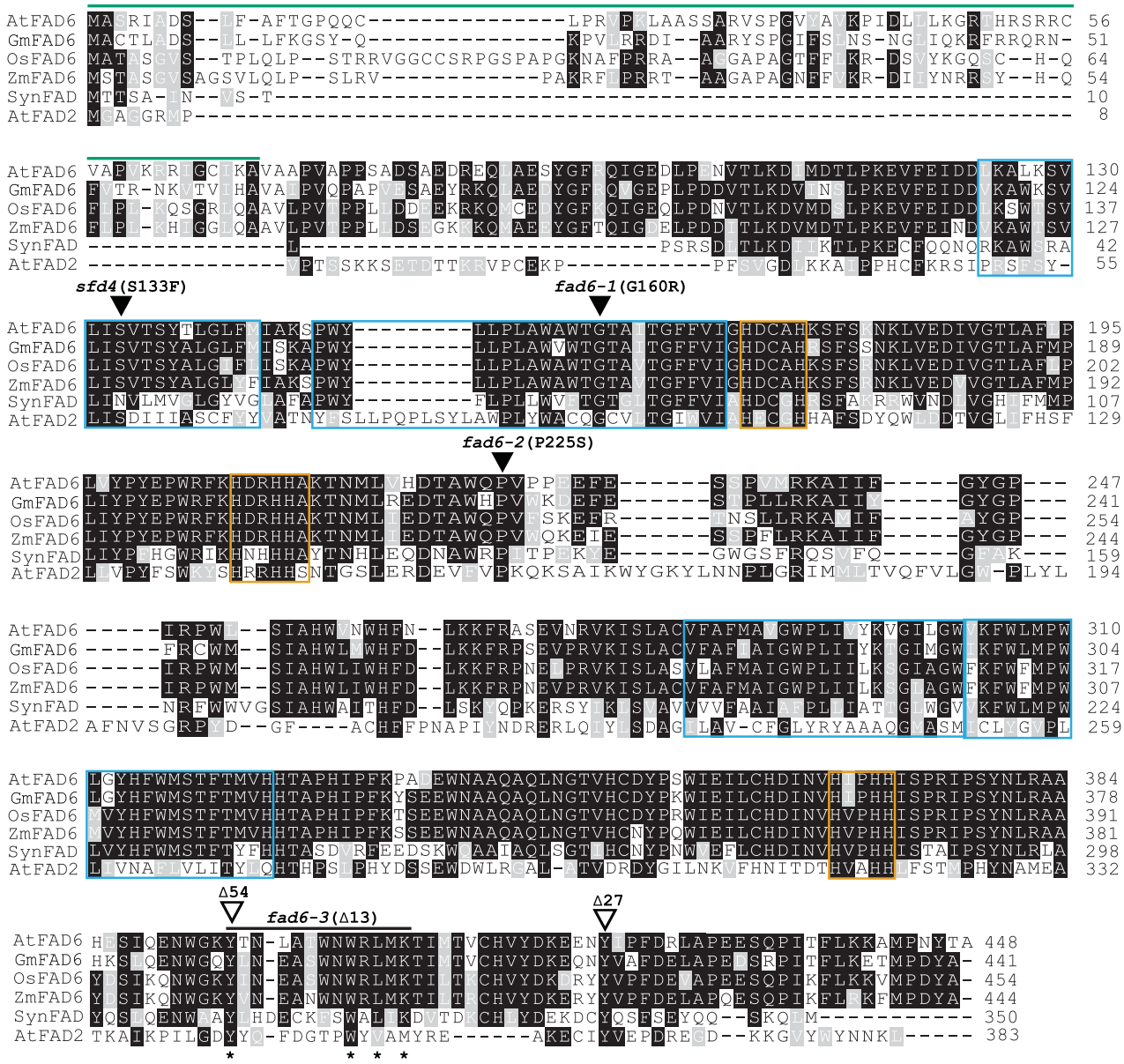

Fig. 3 Amino acid alignments of ω-6 fatty acid desaturases. Amino acid sequences from the FAD2 and FAD6 desaturases from *A. thaliana* were aligned with FAD6 homologs from *Glycine max, Oryza sativa, Zea mays* and *Synechocystis*. Black triangles indicate the positions of mutations in existing Arabidopsis *fad6-1* and *fad6-2* mutant alleles. The black line indicates the 13 amino acids that are deleted in *fad6-3*. Asterisks denote residues deleted in *fad6-3*, conserved in FAD6 homologs and selected for mutagenesis. White triangles indicate the location of C-terminal truncations. The green line indicates the predicted plastidic targeting sequence. Orange boxes indicate conserved histidine boxes found in fatty acid desaturases. Blue boxes indicate the four predicted transmembrane domains.

mutants are essentially identical to each other and to that of the original Salk_109175C line (**Fig. 1** and **Supplementary Fig. S1**).

Multiple amino acid residues within the deleted region in *fad6-3* are conserved among plants

To determine if the amino acid sequence encoded by the region deleted in *fad6-3* was conserved in other plastidial ω-6 desaturases, we compared the Arabidopsis FAD6 amino acid sequence with homologs from other plants. The analysis revealed that multiple amino acids in the deleted sequence are conserved in FAD6 desaturases among Arabidopsis, soybean, maize and rice (**Fig. 3**). Four amino acids in Arabidopsis FAD6 (Y395, W403, L405 and K407) are conserved in the aligned ω-6 desaturases from rice and cyanobacteria (*Synechocystis* sp. PCC 7509). Two of these amino acids, Y395 and W403, are also conserved in the Arabidopsis endoplasmic reticulum (ER)-localized ω-6 desaturase FAD2, which is 24% identical and 49% similar to Arabidopsis FAD6 (**Fig. 3**). There is no significant difference in the levels of *FAD6* transcript in the leaves of *fad6-3* mutants when compared to wild type (**Supplementary Fig. S5**).

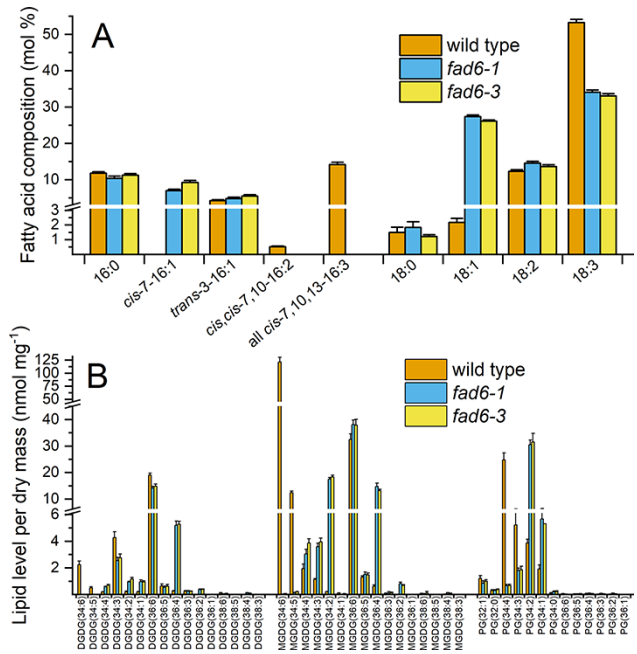

Fig. 4 *fad6-3* mutants exhibit the same lipid phenotype as *fad6-1* mutants. Levels of fatty acids and molecular species of DGDG, MGDG and PG extracted from wild-type, *fad6-1* and *fad6-3* leaf tissue. (A) Fatty acid composition in mole percentage. (B) Levels of molecular species of DGDG, MGDG and PG, where lipid species are indicated as total acyl carbons: total carbon–carbon double bonds. Error bars indicate standard deviation. For each genotype, $n = 6$.

The *fad6-1* mutant also displayed *FAD6* transcript levels similar to those of wild type, perhaps suggesting no regulatory mechanism exists to increase transcriptional expression of the *FAD6* gene in response to decreased polyunsaturation in thylakoid membrane lipids (Falcone et al. 1994).

Mutations in *FAD6* affect desaturase activity and protein stability

Yeast cells expressing codon-optimized versions of *FAD6* were used to quantify the ability of the enzymes encoded by different *FAD6* alleles to desaturate 18:1 to form 18:2. To ensure correct organelle localization in yeast, the chloroplast target sequence was removed and a C-terminal KEKKKNL ER retention motif was added (Venegas-Calerón et al. 2010). A hemagglutinin (HA) epitope tag was added at the N-terminus to enable the detection of the expressed protein. Arabidopsis *FERREDOXIN2* (*FD2*) was co-expressed to act as an electron donor (Venegas-Calerón et al. 2009). Wild-type yeast does not produce 18:2, but the expression of *FAD6* resulted in the synthesis of small but detectable amounts of this polyunsaturated fatty acid (**Supplementary Figs. S6A** and **S7**). Different combinations of promoters controlling the expression of *FAD6* and *FD2* were tested to optimize desaturase activity. The CDC11 constitutive promoter driving *FAD6* and the GAL1/10 galactose inducible promoter driving *FD2* led to the highest production of 18:2 (**Supplementary Fig. S6B**). The length of the induction period was also optimized (**Supplementary Fig. S6C**). Under these optimal conditions, expression of the wild-type *FAD6* resulted in the accumulation of ~0.6 mol% 18:2 in yeast cells (**Fig. 5A**). Immunoblotting for the HA epitope detected a 50-kDa protein, consistent with the predicted size of FAD6.

Versions of FAD6 with mutations corresponding to the different mutant alleles found in Arabidopsis were also expressed in yeast. None of these mutant versions of FAD6 were capable of synthesizing 18:2 (**Fig. 5A**). Strikingly, much lower levels of mutant fad6 protein were detected as compared to the wild-type FAD6. This was particularly true for yeast expressing *fad6-1* and *fad6-2*. Even though fad6-3 protein accumulated to higher levels than the other two mutant proteins, all three mutant protein levels were ~5- to 10-fold lower than that of the wild-type FAD6. The four conserved amino acids encoded by the region deleted in *fad6-3* (**Fig. 3**) were individually mutated to alanine and the effects on activity were tested. While yeast expressing the wild-type FAD6 displayed an average 18:2 content of 0.65 mol%, the alanine-substitution mutants accumulated significantly lower levels of 18:2 (**Fig. 5B**). The W403A and K407A proteins produced 18:2 levels of 0.067 and 0.090 mol%, respectively, higher than the amounts produced by Y395A (0.017 mol%) and L405A (0.021 mol%) but much lower than the 18:2 levels produced by the wild-type FAD6. A fad6 mutant protein with all four of these conserved residues converted to alanine (4A) failed to synthesize 18:2 (**Fig. 5C**). Levels of the 4A FAD6 protein were ~5-fold lower than the wild-type FAD6 but similar to those of the single mutants. Deletions of either the last 27 amino acids (Δ27) or the last 54 amino acids (Δ54) resulted in no production of 18:2 (**Fig. 5C**). In contrast to the missense mutant proteins, protein levels of the C-terminal Δ27 *fad6* protein were nearly as high as the wild-type protein when expressed in yeast.

Modeling suggests the region deleted in fad6-3 interacts with residues near the active site

As shown in **Fig. 3**, FAD6 is predicted to contain four transmembrane domains and three histidine boxes, which form the catalytic site. Two of the histidine boxes are in the loop between the second and third transmembrane helices. The third histidine box (residues 367–371) is in the segment following the 4th transmembrane helix (residues 324–448). 3D modeling of the wild-type FAD6 with the AlphaFold protein structure algorithm produces a high-confidence model, which can be accessed at https://alphafold.ebi.ac.uk/entry/P46312 (**Fig. 6**; Jumper et al. 2021; Varadi et al. 2021). The model predicts that, in the wild-type FAD6, the residues 395–407 occur in a coil–sheet–coil–helix structure. The sheet sequence (residues 397–400) is hydrogen bonded to a parallel sheet sequence (residues 349–352), which lies near the third histidine box, suggesting that the deleted sequence may contribute indirectly to the active site conformation. The same sheet sequence is also predicted to be lying antiparallel and hydrogen bonded to a sheet sequence at residues 94–96 in the

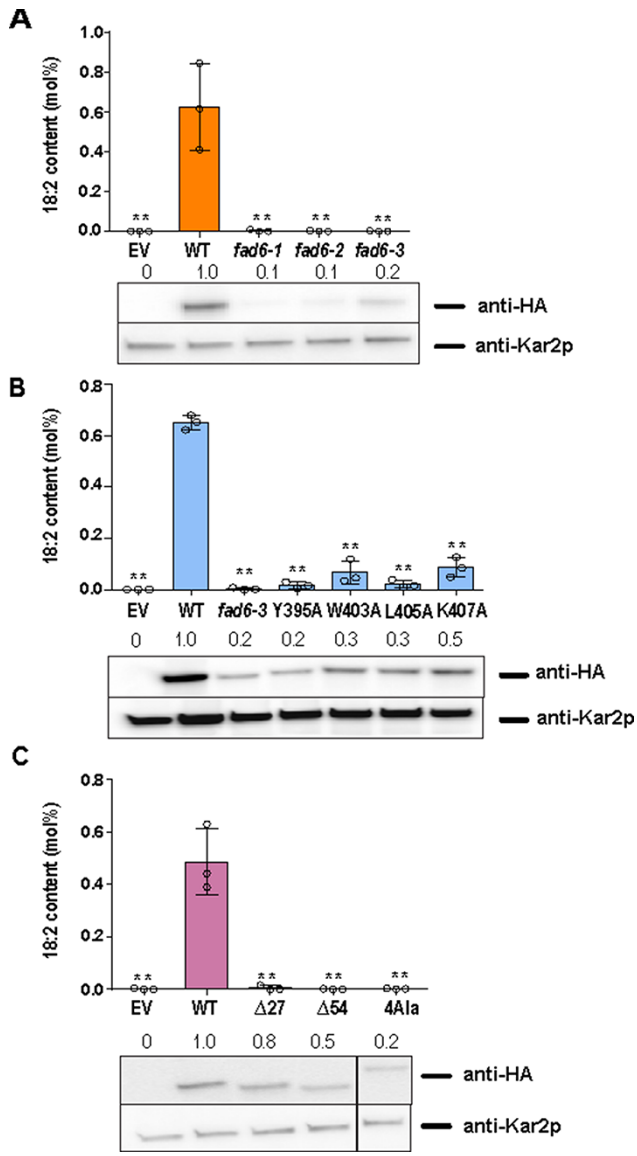

Fig. 5 Mutant fad6 proteins show little or no catalytic activity and are unstable when expressed in yeast. Quantification of 18:2 in total lipid extracts from yeast expressing HA-tagged wild-type FAD6 or mutant fad6 proteins. Immunoblotting using anti-HA and anti-Kar2p antibodies was used to detect and quantify FAD6/fad6 and Kar2p levels, respectively. One representative of three immunoblots is shown. Numbers above each immunoblot indicate FAD6 or fad6 protein accumulation relative to Kar2p normalized to a wild-type protein level of 1. Data represent the mean ± standard deviation of three biological replicates. **, $P < 0.01$ (Student's *t*-test). A. Arabidopsis *fad6* alleles. (B) Single conserved residues mutated to Ala. (C) Deletions and substitutions of residues. Δ27, deletion of 27 C-terminal residues; Δ54, deletion of 54 C-terminal residues; 4A, alanine substitutions in four conserved residues. Superfluous lanes from the Western blots were removed to simplify the figure.

N-terminal portion of the protein. To investigate the impact of the deletion in *fad6-3* and the alanine substitutions on protein structure, the C-terminal portion of the protein was also modeled using Iterative Threading ASSEmbly Refinement (I-TASSER; **Supplementary Fig. S8**; Yang et al. 2015, Yang and Zhang 2015a, 2015b). The modeled portion of the protein was from residue 324, the first residue after the predicted fourth and final transmembrane segment, to the C-terminus. Although the I-TASSER model did not produce a highly confident prediction, its secondary structure predictions are in general agreement with the AlphaFold model. The I-TASSER model also predicts that the 13 amino acids deleted in *fad6-3* (residues 395–407) adopt a coil–strand (residues 398–402)–coil–helix structure in the wild-type FAD6. Both models indicate that, in the wild-type FAD6, the conserved W395, which is absent in *fad6-3* and in the 4A mutant, is in the first coil region, while the helical region starts at W403, and also includes the conserved L405 and K407 (**Supplementary Fig. S8**). I-TASSER modeling predicts that the *fad6-3* deletion not only removes the deleted secondary structural features but also alters the features downstream of the deleted region. On the other hand, the 4A substitution is predicted to remove the initial coil region, extending the preceding helical region to the strand and conceivably altering the orientation of the putatively H-bonded strand area as well as downstream sequences. Overall, modeling suggests that the region deleted in *fad6-3* interacts with multiple other sequences in the protein's three-dimensional structure, and thus, it implies that loss of the region may affect the conformation of the active site.

Discussion

The lipidomic analysis of Arabidopsis mutants represents a resource for future studies

The *fad6-3* mutation was present in the background of Arabidopsis T-DNA insertion line Salk_109175C. The lipid compositional differences between leaves of Salk_109175C and wild-type plants were identified in a lipidomic screen of 364 Salk lines, conducted on plants harvested and analyzed without treatment and after wounding treatment. The plants were grown directly from seeds received from ABRC (Ohio State University, Columbus, Ohio, USA), without additional genetic analysis. The data, presented in **Supplementary Tables S1–S10**, with the lines most different from wild-type plants in leaf lipid composition identified in **Table 1**, provide an overview of the lipid composition of each line and may serve as an aid for scientists choosing lines or genes of interest for further analysis.

A new *fad6* mutant allele displays altered lipid composition

In this study, we used lipid profiling and mapping based on nucleotide polymorphisms to identify a new mutant allele of *FAD6*, which encodes a plastid-localized ω-6 fatty acid desaturase that introduces a second double bond to monounsaturated fatty acids esterified in galactolipids. The *fad6-3* mutant possesses the same leaf lipid phenotype, including lower levels of MGDG(18:3/16:3) relative to MGDG(18:3/18:3), as the previously identified *fad6-1* mutant (**Fig. 4**). Both mutants have

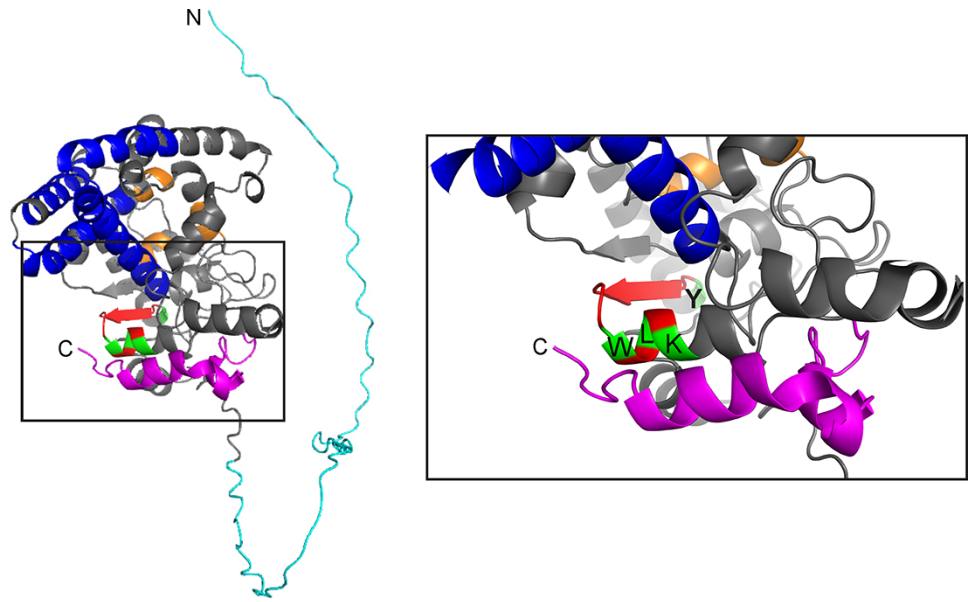

Fig. 6 The predicted 3D structure of the *A. thaliana* FAD6 protein. Model of the FAD6 protein from the AlphaFold Monomer v2.0 pipeline (Jumper et al. 2021, Varadi et al. 2021). Helices and strands are predicted with a very high per-residue confidence score (pLDDT > 90). Plastidic targeting sequence at the N-terminus, light blue; transmembrane helices, blue; histidine boxes, orange. Magnification of the C-terminal region is shown in the box. The 27-amino-acid C-terminal deleted region is shown in magenta. The 13-amino-acid deleted segment is shown in red and green. The four conserved amino acids (Y395, W403, L405 and K407) are indicated in green. Images were created by the PyMOL Molecular Graphics System, Version I.2r3pre, Schrödinger, LLC.

very low levels of plastidic lipids containing 16:2 and 16:3, which are synthesized only in the plastid and must be desaturated via FAD6 (Falcone et al. 1994, Xu et al. 2010; **Fig. 4A**). Although FAD6 produces 18:2, as well as 16:2, levels of 18:2 and 18:3 are much less affected than 16:2 and 16:3 in the *fad6* mutants (**Fig. 4A**). This is because 18:2 is also formed in the ER by FAD2, another ω-6 fatty acid desaturase that acts primarily on 18-carbon substrates in planta. ER-synthesized, 18-carbon polyunsaturated fatty acids can be imported into the plastid and incorporated in plastidic lipids, such as MGDG and DGDG, as well as used to assemble extraplastidically produced lipids, such as PC and PE. The production of 18:2 and 18:3 through the ER desaturation pathway in *fad6* mutants results in PC and PE molecular species profiles that are only slightly altered compared to those of wild-type plants (**Supplementary Fig. S4**). On the other hand, MGDG and DGDG in *fad6* lack species containing 16:3, particularly 18:3/16:3, which is prominent in wild-type plants (**Fig. 4B**). Eighteen-carbon polyunsaturated fatty acids imported from the ER to the plastid are incorporated readily into MGDG and DGDG, which contain wild type or slightly higher levels of 18:3/18:3 species in the *fad6* mutants compared to wild-type plants. However, 18:3 is not readily incorporated into PG, which has very much lower levels of PG(34:4), i.e. PG(18:3/*trans*-3-16:1), in the *fad6* mutants than in wild-type plants (**Fig. 4B**). This is consistent with previous data indicating that PG contains only fatty acids that never leave the plastid, whereas MGDG and DGDG can incorporate fatty acids (or diacylglycerol backbones) desaturated in the ER (Roughan 1985, Fritz et al. 2007).

A secondary mutation causes the observed lipid phenotype in a T-DNA mutant line

The *fad6-3* mutation was derived from the T-DNA insertion line Salk_109175C, which contains a T-DNA insertion in *At5g64790*, a gene encoding a putative *O*-glycosyl hydrolase. Multiple pieces of evidence demonstrate that the lipid phenotype of the original mutant line is caused by a mutation in *FAD6* and not the T-DNA insertion in *At5g64790*. First, the lipid phenotype is consistent with a loss of ω-6 fatty acid desaturase activity in the chloroplast, similar to that in other *fad6* mutant alleles (**Fig. 4**; Falcone et al. 1994; Xu et al. 2010). Additionally, *At5g64790* is strongly expressed in pollen but not leaves, whereas the lipid phenotype of Salk_109175C is observed in leaves, where *FAD6* is expressed (**Fig. 1A**; **Supplementary Fig. S5**). Crucially, the altered levels of MGDG do not segregate with the T-DNA insertion in *At5g64790* (**Fig. 1B**). Instead, the phenotype maps to the region of chromosome 4 that contains *FAD6* (**Fig. 2**). Sequencing of the *FAD6* locus and cDNA revealed a G to A nucleotide change that affects a splice acceptor site, causing an in-frame deletion of the first 13 amino acids of exon 10 near the C-terminus of the encoded protein (**Fig. 2**, **Supplementary Fig. S3**). This deletion results in a nonfunctional desaturase enzyme in a yeast heterologous expression system (**Fig. 5**). The discovery that the mutant phenotype of Salk_109175C is not caused by the T-DNA insertion in *At5g64790* provides yet another example in which a secondary mutation is responsible for the mutant phenotype of a T-DNA insertion line. Phenotypes that are not linked to T-DNA insertion are well documented (Ajjawi et al. 2010, Wilson-Sánchez et al. 2014),

and they illustrate the importance of providing additional evidence beyond a phenotype in only one mutant line to demonstrate a function of a gene.

The C-terminus of FAD6 is required for protein function

The splice-site mutation in *fad6-3* removes 13 amino acids (residues 395–407) from the C-terminal region, resulting in a mutant protein that lacks catalytic activity (**Fig. 5A**). To test the notion that the deletion of this segment caused a conformational change in the FAD6 C-terminus that introduced an interfering downstream piece of the protein to protein's active site, larger deletions were made. However, proteins with larger deletions of the C-terminus failed to restore FAD6 activity (**Fig. 5C**), indicating that the C-terminal region itself is required for the proper structure and/or function of FAD6.

Of the 13 amino acids deleted in the fad6-3 mutant protein, four are conserved in FAD6 homologs from other species, including cyanobacteria (**Fig. 3**). Of these four conserved amino acids, two (Y395 and W403) are also conserved in another Arabidopsis ω-6 fatty acid desaturase, FAD2. The other two residues (L405 and K407) are replaced by similar amino acids in FAD2, suggesting the importance of the four amino acids for protein structure and/or function. To better understand the function of the deleted region, FAD6 variants, where one or all four of the conserved residues were replaced with alanine, were examined. Individual substitutions result in large reductions in enzyme activity and protein stability (**Fig. 5B**). Mutation of all four conserved residues completely abolished desaturase activity (**Fig. 5C**), indicating non-redundant roles for each residue. Residues in the C-terminus may be important in the proper folding and thus stability of the protein or, as suggested by modeling, in orienting or stabilizing the catalytic site. Indeed, deletions of the C-terminus both eliminate enzyme activity and reduce protein stability, although it is intriguing that the deletion of last 34 residues results in higher protein stability compared to all the other mutations (**Fig. 5C**). According to the I-TASSER secondary structure prediction (**Supplementary Fig. 8**), the Δ27 mutant protein retains a helical region with high thermal stability in the wild-type protein, whereas deletion of the 54-terminal amino acids removes this helix. Taken together, the results suggest the critical importance of the C-terminus of FAD6 in interacting with other parts of the enzyme. However, a more definitive understanding of FAD6 C-terminal and its influence on the active site will require the structural analysis of the entire protein, which is a nontrivial task given the presence of four transmembrane sequences.

Materials and Methods

Plant materials, growth conditions and wounding treatment

Seeds of *Arabidopsis thaliana* accession Col-0, Ler-0 and lines with T-DNA insertions, including Salk_109175C, were obtained from ABRC. Seeds were sown at 3 seeds per well in 72-well plug trays (Hummert International, Earth City, MO, USA) filled with loosely packed, autoclaved and cooled Pro-Mix 'PGX' soil (Hummert International) saturated with 0.01% Jacks All Purpose 20-20-20 fertilizer (J.R. Peters Inc., Allentown, PA, USA). After trays were sown, they were covered with propagation dome lids and incubated at 4°C for 2 days before transfer to a growth chamber under a 14/10 h light/dark cycle at 21°C with 60% humidity. Light intensity was maintained at 80–100 μmol photons $m^{-2}s^{-1}$. Propagation dome lids were used to cover the plants for the first 9 d to maintain high humidity. Trays were watered on days 11, 16, 24 and 28. On day 13 after sowing, plants were thinned to one plant per well. On day 20, trays were fertilized again with 0.01% Jacks All Purpose 20-20-20 fertilizer (J.R. Peters, Inc.). At 30 d of age, leaf 4 was harvested for lipid analysis.

For the Salk line screening experiment, confirmed homozygous Salk lines with a Col-0 background (Alonso et al. 2003) were obtained from ABRC and were used without further genetic analysis. Lines were planted in randomized designs on each of three 72-well trays with one of each line and four Col-0 plants per tray. Three trays planted with replicate accessions are designated as a 'day', and the wild-type Col-0 plants on the same trays are the control plants for comparison of lipid profiles.

A line derived from Salk_109175C, homozygous for the insertion in *At5g64790* but lacking the *fad6-3* mutation, was donated to ABRC by H.L. and R.W. and is available as stock number CS72295. The *fad6-3* mutant will be donated upon acceptance of this manuscript.

When plants were subjected to wounding treatment, leaf 5 was wounded immediately after the harvest of leaf 4. Wounding was performed with a hemostat, across the midvein, 2–3 times on leaf 5. The same leaf was harvested 45 min later.

Lipid extraction and instrument parameters for analyses

Extraction and the lipid analytical procedure for broad-based lipid analysis using multiple reaction monitoring were performed as described by Vu et al. (2014) and Shiva et al. (2018), including the use of quality control samples for normalization of lipid profiles among data collected on different dates. The mass spectral settings for specific lipids, identified by 'lipid numbers', are available in the supplemental data of Vu et al. (2014) and Shiva et al. (2018). The global settings for those analyses on the Xevo TQ-S (Waters Corporation, Milford, MA, USA) mass spectrometer were identical to those reported by Vu et al. (2014). In most cases, lipid amounts are presented as normalized intensity per milligram (or 0.04 mg for **Supplementary Tables S2** and **S3**) of leaf dry mass, where a signal of 1 corresponds to the same amount of signal as derived from 1 nmol or 1 pmol of internal standard(s), as indicated in the figure legends. In other cases (**Figs. 1B** and **4** and **Supplementary Fig. S2**), neutral loss and precursor scans were used, as described by Xiao et al. (2010). **Fig. 1B** data are presented as a ratio of the signals of two lipid species, while data in **Fig. 4** and **Supplementary Fig. S2** were corrected with response factors for galactolipid species to represent true lipid amounts (nmol) per dry weight (mg).

Analysis of lipid profile data from screening of mutant lines

Lipid levels from unwounded and wounded plants, presented as both normalized intensity per milligram of leaf dry mass, where a signal of 1 corresponds to the same amount of signal as derived from 1 pmol of internal standard(s) and as percentage of total lipid normalized intensity, were compared with the unwounded or wounded wild-type samples on the same trays (trays with the same 'day' designation), using a *t*-test without correction for multiple testing. The lipids or lipid classes with *P* values less than 0.05, 0.01, 0.001 and 0.0001 in the comparison of each Salk line vs. wild-type were enumerated separately for amount data from unwounded plants, amount data from wounded plants, percentage data from unwounded plants and percentage data from wounded plants. The *P* values calculated from the amount data and the *P* values calculated from the percentage data were used to calculate a score for the difference

between lipids from unwounded lines and those from unwounded, wild-type plants, and similarly, a score was calculated for the difference between lipids from wounded lines and those from wounded, wild-type plants. First, the number of lipids different in each line, compared to the same lipids in wild type, at *P*-values of 0.05, 0.01, 0.001, and 0.0001 were enumerated (**Supplementary Tables S6-S9**). After subtracting the expected number of positive counts due to random chance (number of lipids analyzed × the *P* value cutoff) from each *P* value count, the score was calculated as the sum of the remaining counts <0.05 × 1, the remaining counts <0.01 × 5, the remaining counts <0.001 × 50 and the remaining counts <0.0001 × 500. The scores for lipids from unwounded and wounded plants were combined to get an overall score for the difference of the Salk line's lipid composition from that of wild-type plants (**Supplementary Table S10**).

Genetic analysis of wild-type Col-0 × Salk_109175C F2

DNA was extracted from leaf 5 of 30-day-old wild-type (Col-0) Arabidopsis and Salk_109175C plants using the protocol described in Edwards et al. (1991). Primers for sequencing, amplification and reverse transcription - quantitative polymerase chain reaction (RT-qPCR) are listed in **Supplementary Table S15**. Plants were genotyped as wild type, heterozygous or homozygous for the known T-DNA insertional mutation using Econotaq polymerase chain reaction (PCR) master mix (Lucigen, Middleton, WI) and the primers Salk_109175C-F, Salk_109175C-R and LBb1.3 (**Supplementary Table S15**).

Mapping

Mapping based on nucleotide polymorphisms (i.e. map-based cloning) was achieved by crossing the mutant (Col-0 accession) to L*er*-0, creating an F2 mapping population and following the mapping procedure outlined by Lukowitz et al. (2000). Sequences for flanking PCR markers were obtained from the Arabidopsis Mapping Platform (Hou et al. 2010). Oligonucleotides used for mapping are listed in **Supplementary Table S16**.

Amplification and sequencing of *FAD6*

The full-length genomic *FAD6* was amplified from wild-type (Col-0) and *fad6*-3 DNA extracted from leaves using Phusion High-Fidelity DNA Polymerase (Thermo Fisher Scientific, Waltham, MA, USA) with the primers FAD6 5′UTR-F and FAD6 3′UTR-R (**Supplemental Table S15**). After amplification, PCR products were gel purified before being sequenced with the primers FAD6seq1, FAD6seq2, FAD6seq3, FAD6seq4 and FAD6seq5. FAD6 cDNA was amplified and sequenced using the same methods and primers as for the genomic DNA.

Quantification of *FAD6* gene expression

To grow plants for RNA extraction, Arabidopsis seeds were surface sterilized by chlorine gas treatment and sown onto 0.8% agar (plant tissue culture grade) containing 1× Murashige and Skoog medium (Murashige and Skoog 1962), 1% sucrose and 0.5% 2-Morpholinoethanesulfonic acid (MES) buffer at pH 5.8. Seeds were transferred to 21°C and grown under continuous light for 12 days, at which time they were transferred to 72-well plug trays (Hummert International) filled with loosely packed, autoclaved and cooled Pro-Mix 'PGX' soil (Hummert International) saturated with 0.01% Jacks All Purpose 20-20-20 fertilizer (J.R. Peters, Inc.) and grown for another 18 days. Plants were watered on days 16, 24 and 28 and fertilized on day 20. Leaf tissue samples for RNA extraction were taken on day 30. Tissue samples were taken from leaf 5 of 30-day-old wild-type (Col-0) and *fad6*-3 plants. Tissue samples were frozen in liquid nitrogen and stored at −80°C prior to RNA extraction with the RNeasy Plant Mini Kit and on-column RNase-Free DNase Set (Qiagen, Hilden, Germany). Total RNA (0.5 μg) was used as a template for cDNA synthesis. The first-strand cDNA synthesis was performed with Oligo (dT) primer using GoScript Reverse Transcriptase (Promega, Madison, WI, USA). Real-time PCR was performed using iTaq SYBR Green Supermix with the CFX96 Touch Real-Time PCR Detection System (Bio-Rad Laboratories, Inc.). Each reaction contained 10 μl of SYBR Green Supermix, 1 μl of forward and reverse 10 mM gene-specific primers and 5 μl of cDNA (diluted 5-fold) in 20 μl. Standard curves were generated from 10-fold dilutions of amplicons for each primer pair. *ACT7* served as the reference gene. The qPCRFAD6-F, qPCRFAD6-R, ACT7-F and ACT7-R gene-specific primers (**Supplemental Table S15**) were used for PCR amplification of *FAD6* and *ACT7*, respectively.

Sequence alignments and structural modeling

Alignment of amino acid sequences for ω6-desaturase proteins was done using Clustal X v.2.094 with the default setting. Protein structural modeling was done using I-TASSER (Yang et al. 2015, Yang and Zhang 2015a, 2015b).

Arabidopsis FAD6 and FD2 plasmid construction

The FAD6 protein sequence lacking the chloroplast transit peptide, with added residues KEK-KKNL (for ER localization) and an N-terminal HA tag, and the FD2 protein sequence were codon-optimized for expression in *Saccharomyces cerevisiae* and synthesized by GenScript (GenScript, Piscataway, NJ, USA). Plasmids used in this study are listed in **Supplementary Table S17**. For plasmid construction, plasmids pRS31699 and pRS31599 were digested with *SpeI* and *NotI* (New England Biolabs, Ipswich, MA, USA), respectively. The general strategy for strain construction was to use in vivo ligation and homologous recombination (Muhlrad et al. 1992, Kitazono 2009, Bessa et al. 2012, Finnigan and Thorner 2015) to generate a plasmid containing the gene of interest (or an epitope-protein-tagged derivative) under the control of a promoter and terminator of choice (Gal1/10 or CDC11) and harboring a juxtaposed MX-based drug cassette (Goldstein and McCusker 1999). Oligonucleotides used to amplify fragments for in vivo ligation are listed in **Supplementary Table S18**.

Functional expression in yeast

Yeast strains, listed in **Supplementary Table S19**, were grown at 30°C in synthetic dextrose (SD) medium supplemented with the appropriate amino acids and/or other nutrients and glucose (2%) as the carbon source. Where indicated, galactose (2%) was the carbon source. The generated plasmids were transformed into the *S. cerevisiae* strain INVSc1 (Invitrogen, Carlsbad, CA, USA) using the lithium acetate method (Elble 1992). Transformed yeast cells were grown at 30°C in synthetic media (SD-Ura-Leu) supplemented with the appropriate amino acids. Expression of the transgenes was induced by the addition of galactose to 2% (w/v). Cell pellets were suspended in a single phase mixture consisting of 0.8 parts water, 1 part chloroform and 2 parts methanol containing 50 μg (65.3 nmol) TAG(15:0/15:0/15:0). Cells were lysed by vortexing for 5 min with ∼500 μl of 0.5-mm-diameter zirconia/silica beads (BioSpec Products, Inc., Bartlesville, OK, USA). Chloroform (one part) and water (one part) were added to split phases, and samples were vortexed and then centrifuged for 10 min. The organic lower layer was removed and saved. Chloroform (one part) was added to the aqueous layer, samples were vortexed and centrifuged and the lower layer was removed and combined with the previously saved organic layer; this was done two times. The combined lower layers were used for gas chromatography (GC) analysis as fatty acid methyl esters (FAMEs).

Analysis of fatty acids by GC

FAMEs were prepared and analyzed by the method described by Christie (1982) with minor modifications. About 0.5–1 mg of dry lipid extract was placed in glass tubes with Teflon-lined screw caps. The solvent was evaporated under a nitrogen stream. One milliliter of 3 M methanolic HCl was added to each sample, and each was bubbled with nitrogen gas. The samples were incubated for 30 min at 78°C. Two milliliters of HPLC-grade water was added, and FAMEs were extracted twice with 2 ml of hexane. The solvent was evaporated, and the FAMEs were redissolved in 70 μl of hexane. FAME analysis was performed on an

Agilent 6890N gas chromatograph (Santa Clara, CA, USA) coupled to a flame ionization detector (FID). A DB-23 (60 m × 0.25 mm × 0.25 μm) column was installed. An Agilent 7683 autosampler was used to inject 3 μl of sample in splitless mode. The carrier gas was helium with a flow rate of 1.5 ml min^{-1}. The oven temperature was maintained at 150°C for 1 min, ramped to 175°C at 25°C/min, ramped to 230°C at 4°C/min, and held at 230°C for 8 min. The total run time was 23.75 min. The FID detector was operated at 260°C. The hydrogen flow to the detector was 30 ml/min, and airflow was 400 ml/min. The sampling rate of the FID was 20 Hz.

FAMEs were identified by comparing their retention times with FAMEs in a standard mixture. The 15:0 internal standard was used to quantify the amount of individual fatty acid. Fatty acid composition was expressed as percentage of dry weight.

GC-MS analysis for confirmation of the linoleic acid methyl ester structure

GC-mass spectrometry (MS) was used for confirmation of the *cis,cis*-9,12-18:2 methyl ester structure in yeast expressing Arabidopsis FAD6 and was performed on an Agilent 6890N GC coupled to an Agilent 5975N quadrupole mass selective detector. The GC was fitted with a VF-5MS capillary column (inert 5% phenylmethyl column, length: 30 mm, internal diameter: 250 μm and film thickness: 0.25 μm) with a 10-m EZ-Guard column. Helium was used as the carrier gas at a column flow rate of 1 ml/min. The front inlet was operated at 250°C. The Agilent 7683 autosampler was used to inject 1 μl of the sample in the splitless mode. The GC oven temperature program was as follows: initial temperature of 120°C, held for 1 min and increased at 5°C/min to 290°C. The total run time was 35 min. The mass spectrometer was operated in the electron impact mode at 70 eV ionization energy. The MS quad temperature was 150°C, and the MS source temperature was 230°C. The data acquisition was in scan mode. The scanned range was *m/z* 50–650. The data were processed with Agilent ChemStation software.

Immunoblot detection of recombinant FAD6 protein in yeast

Total protein was extracted from yeast using a method employing sodium hydroxide–trichloroacetic acid (Knop et al. 1999), resuspended in 250 μl of protein storage buffer (20 mM Tris–HCl, pH 6.87 and 1% glycerol) and quantified using a bicinchoninic acid assay kit (ThermoFisher Scientific). Eight micrograms of total protein was incubated in 2× sample buffer (120 mM Tris–HCl, pH 6.8, 5% glycerol, 8 M urea, 10% β-mercaptoethanol and 8% sodium dodecyl sulfate (SDS) SDS) at 37°C for 30 min and then loaded onto a 10% SDS-polyacrylamide gel electrophoresis (PAGE) gel (GenScript ExpressPlus PAGE Gel). After electrophoretic separation, proteins were transferred to nitrocellulose membranes, which were split at the ∼80 kDa size mark to allow Karyogamy2 (Kar2; a yeast ER-localized ATPase) and FAD6-HA to have their own blots. After blocking for 1 h, a 1:5,000 dilution of anti-HA antibody (clone 2-2.2.2.14; Thermo Scientific) or anti-Kar2p (clone sc-33630; Santa Cruz Biotechnology) in phosphate-buffered saline with Tween-20 was added and incubated for 24 h at 4°C. After washing off unbound antibodies, a 1:5,000 dilution of goat anti-mouse Immunoglobulin G (IgG) horseradish peroxidase (HRP)-conjugated (Southern Biotech) or goat anti-rabbit IgG HRP-conjugated (Santa Cruz Biotechnology) secondary antibody was added and allowed to incubate at room temperature for 1 h. Bound antibodies were detected using the SuperSignal West Femto Maximum Sensitivity Substrate kit (ThermoFisher Scientific) on a c500 Azure Biosystems imaging instrument. Band intensities from immunoblots were quantified using ImageQuant. Relative band intensity was calculated by normalizing anti-HA intensity to the anti-Kar2p intensity.

Supplementary Data

Supplementary data are available at *PCP* online.

Data Availability

The data underlying this article are available in the article and in its online supplementary material.

Funding

National Science Foundation (MCB-1413036 to R.W., MCB-1412942 to J.S. and MCB-1616818 to K.S.); United States Department of Agriculture National Institute of Food and Agriculture, Hatch/Multi-State project (1013013 to R.W., K.S. and T.P.D.); Undergraduate Research Award from the Kansas State University College of Arts and Sciences (to H.L.); STAR and semester scholar awards to H.L. and M.C. from the Kansas IDeA Network of Biomedical Research Excellence funded by an Institutional Development Award (IDeA) from the National Institute of General Medical Sciences of the National Institutes of Health (P20GM103418); Ronald E. McNair Postbaccalaureate scholarship from Achievement Program at Kansas State University, a federally funded TRIO Program through the United States Department of Education (P217A120223 to H.L.); Kansas Lipidomics Research Center, where instrument acquisition was funded by National Science Foundation (EPS 0236913, DBI 0521587, DBI1228622 and DBI 1726527); Kansas Technology Enterprise Corporation; Kansas IDeA Network of Biomedical Research Excellence funded by an IDeA from the National Institute of General Medical Sciences of the National Institutes of Health (P20GM103418); Kansas State University; Kansas Agricultural Experiment Station (22-262-J).

Acknowledgements

The authors are grateful to Dr. Zulkarnain Chowdhury for his guidance in mapping the gene, to Dr. Sujon Sarowar for help with primer design, to Dr. Gregory Finnigan for direction and oversight of the yeast in vivo ligation method and to Dr. Prasad Parchuri for other valuable molecular biology-related advice. Mass spectral analysis was carried out at the Kansas Lipidomics Research Center.

Disclosures

The authors have no conflicts of interest to declare.

References

Ajjawi, I., Lu, Y., Savage, L.J., Bell, S.M. and Last, R.L. (2010) Large-scale reverse genetics in Arabidopsis: case studies from the Chloroplast 2010 Project. *Plant Physiol.* 152: 529–540.

Alonso, J.M., Stepanova, A.N., Leisse, T.J., Kim, C.J., Chen, H., Shinn, P., et al. (2003) Genome-wide insertional mutagenesis of *Arabidopsis thaliana*. *Science* 301: 653–657.

Bessa, D., Pereira, F., Moreira, R., Johansson, B. and Queirós, O. (2012) Improved gap repair cloning in yeast: treatment of the gapped vector with Taq DNA polymerase avoids vector self-ligation. *Yeast* 29: 419–423.

Browse, J., Kunst, L., Anderson, S., Hugly, S. and Somerville, C. (1989) A mutant of Arabidopsis deficient in the chloroplast 16:1/18:1 desaturase. *Plant Physiol.* 90: 522–529.

Carlsson, A.S., LaBrie, S.T., Kinney, A.J., Von Wettstein-Knowles, P. and Browse, J. (2002) A KAS2 cDNA complements the phenotypes of the Arabidopsis fab1 mutant that differs in a single residue bordering the substrate binding pocket. *Plant J.* 29: 761–770.

Christie, W.W. (1982) Lipid Analysis, 2nd edn. pp. 52–53. Pergamon Press, Oxford.

Edwards, K., Johnstone, C. and Thompson, C. (1991) A simple and rapid method for the preparation of plant genomic DNA for PCR analysis. *Nucleic Acids Res.* 19: 1349.

Elble, R. (1992) A simple and efficient procedure for transformation of yeasts. *BioTechniques* 13: 18–20.

Falcone, D.L., Gibson, S., Lemieux, B. and Somerville, C. (1994) Identification of a gene that complements an Arabidopsis mutant deficient in chloroplast omega 6 desaturase activity. *Plant Physiol.* 106: 1453–1459.

Falcone, D.L., Ogas, J.P. and Somerville, C.R. (2004) Regulation of membrane fatty acid composition by temperature in mutants of Arabidopsis with alterations in membrane lipid composition. *BMC Plant Biol.* 4: 17.

Finnigan, G.C. and Thorner, J. (2015) Complex in vivo ligation using homologous recombination and high-efficiency plasmid rescue from *Saccharomyces cerevisiae*. *Bio. Protoc.* 5: e1521.

Fritz, M., Lokstein, H., Hackenberg, D., Welti, R., Roth, M., Zähringer, U., et al. (2007) Channeling of eukaryotic diacylglycerol into the biosynthesis of plastidial phosphatidylglycerol. *J. Biol. Chem.* 282: 4613–4625.

Gao, J., Wallis, J.G. and Browse, J. (2015) Mutations in the prokaryotic pathway rescue the *fatty acid biosynthesis1* mutant in the cold. *Plant Physiol.* 169: 442–452.

Goldstein, A.L. and McCusker, J.H. (1999) Three new dominant drug resistance cassettes for gene disruption in *Saccharomyces cerevisiae*. *Yeast* 15: 1541–1553.

Hou, X., Li, L., Peng, Z., Wei, B., Tang, S., Ding, M., et al. (2010) A platform of high-density INDEL/CAPS markers for map-based cloning in Arabidopsis. *Plant J.* 63: 880–888.

Hugly, S. and Somerville, C. (1992) A role for membrane lipid polyunsaturation in chloroplast biogenesis at low temperature. *Plant Physiol.* 99: 197–202.

Jumper, J., Evans, R., Pritzel, A., Green, T., Figurnov, M., Ronneberger, O., et al. (2021) Highly accurate protein structure prediction with AlphaFold. *Nature* 596: 583–589.

Kachroo, A., Lapchyk, L., Fukushige, H., Hildebrand, D., Klessig, D. and Kachroo, P. (2003) Plastidial fatty acid signaling modulates salicylic acid- and jasmonic acid-mediated defense pathways in the Arabidopsis *ssi2* mutant. *Plant Cell* 15: 2952–2965.

Kitazono, A.A. (2009) Improved gap-repair cloning method that uses oligonucleotides to target cognate sequences. *Yeast* 26: 497–505.

Knop, M., Siegers, K., Pereira, G., Zachariae, W., Winsor, B., Nasmyth, K., et al. (1999) Epitope tagging of yeast genes using a PCR-based strategy: more tags and improved practical routines. *Yeast* 15: 963–972.

Lukowitz, W., Gillmor, C.S. and Scheible, W.R. (2000) Positional cloning in Arabidopsis. Why it feels good to have a genome initiative working for you. *Plant Physiol.* 123: 795–805.

Muhlrad, D., Hunter, R. and Parker, R. (1992) A rapid method for localized mutagenesis of yeast genes. *Yeast* 8: 79–82.

Murashige, T. and Skoog, F. (1962) A revised medium for rapid growth and bio assays with tobacco tissue cultures. *Physiol. Plant.* 15: 473–479.

Nandi, A., Krothapalli, K., Buseman, C.M., Li, M., Welti, R., Enyedi, A., et al. (2003) Arabidopsis *sfd* mutants affect plastidic lipid composition and suppress dwarfing, cell death, and the enhanced disease resistance phenotypes resulting from the deficiency of a fatty acid desaturase. *Plant Cell* 15: 2383–2398.

Roughan, P.G. (1985) Phosphatidylglycerol and chilling sensitivity in plants. *Plant Physiol.* 77: 740–746.

Scherer, G.F.E., Ryu, S.B., Wang, X., Matos, A.R. and Heitz, T. (2010) Patatin-related phospholipase A: nomenclature, subfamilies and functions in plants. *Trends Plant Sci.* 15: 693–700.

Schmidt, H., Dresselhaus, T., Buck, F. and Heinz, E. (1994) Purification and PCR-based cDNA cloning of a plastidial n-6 desaturase. *Plant Mol. Biol.* 26: 631–642.

Schmidt, H. and Heinz, E. (1990) Desaturation of oleoyl groups in envelope membranes from spinach chloroplasts. *Proc. Natl. Acad. Sci. USA* 87: 9477–9480.

Schmidt, H. and Heinz, E. (1993) Direct desaturation of intact galactolipids by a desaturase solubilized from spinach (*Spinacia oleracea*) chloroplast envelopes. *Biochem. J.* 289: 777–782.

Shiva, S., Enninful, R., Roth, M.R., Tamura, P., Jagadish, K. and Welti, R. (2018) An efficient modified method for plant leaf lipid extraction results in improved recovery of phosphatidic acid. *Plant Methods* 14: 14.

Varadi, M., Anyango, S., Deshpande, M., Nair, S., Natassia, C., et al. (2021) AlphaFold Protein Structure Database: massively expanding the structural coverage of protein-sequence space with high-accuracy models. *Nucleic Acids Res.* 50: D439–D444.

Venegas-Calerón, M., Beaudoin, F., Garcés, R., Napier, J.A. and Martínez-Force, E. (2010) The sunflower plastidial omega3-fatty acid desaturase (HaFAD7) contains the signalling determinants required for targeting to, and retention in, the endoplasmic reticulum membrane in yeast but requires co-expressed ferredoxin for activity. *Phytochemistry* 71: 1050–1058.

Venegas-Calerón, M., Youssar, L., Salas, J.J., Garcés, R. and Martínez-Force, E. (2009) Effect of the ferredoxin electron donor on sunflower (*Helianthus annuus*) desaturases. *Plant Physiol. Biochem.* 47: 657–662.

Vu, H.S., Shiva, S., Roth, M.R., Tamura, P., Zheng, L., Li, M., et al. (2014) Lipid changes after leaf wounding in *Arabidopsis thaliana*: expanded lipidomic data form the basis for lipid co-occurrence analysis. *Plant J.* 80: 728–743.

Wilson-Sánchez, D., Rubio-Díaz, S., Muñoz-Viana, R., Pérez-Pérez, J.M., Jover-Gil, S., Ponce, M.R., et al. (2014) Leaf phenomics: a systematic reverse genetic screen for Arabidopsis leaf mutants. *Plant J.* 79: 878–891.

Winter, D., Vinegar, B., Nahal, H., Ammar, R., Wilson, G.V. and Provart, N.J. (2007) An 'electronic Fluorescent Pictograph' browser for exploring and analyzing large-scale biological data sets. *PLoS One* 2: e718.

Xiao, S., Gao, W., Chen, Q.F., Chan, S.W., Zheng, S.X., Ma, J., et al. (2010) Overexpression of Arabidopsis acyl-CoA binding protein ACBP3 promotes starvation-induced and age-dependent leaf senescence. *Plant Cell* 22: 1463–1482.

Xu, C., Moellering, E.R., Muthan, B., Fan, J. and Benning, C. (2010) Lipid transport mediated by Arabidopsis TGD proteins is unidirectional from the endoplasmic reticulum to the plastid. *Plant Cell Physiol.* 51: 1019–1028.

Yang, J., Wang, Y. and Zhang, Y. (2016) ResQ: an approach to unified estimation of B-factor and residue-specific error in protein structure prediction. *J. Mol. Biol.* 428: 693–701.

Yang, J., Yan, R., Roy, A., Xu, D., Poisson, J. and Zhang, Y. (2015) The I-TASSER Suite: protein structure and function prediction. *Nat. Methods* 12: 7–8.

Yang, J. and Zhang, Y. (2015a) I-TASSER server: new development for protein structure and function predictions. *Nucleic Acids Res.* 43: W174–W181.

Yang, J. and Zhang, Y. (2015b) Protein structure and function prediction using I-TASSER. *Curr. Protoc. Bioinf.* 52: 5.8.1–5.8.15.

Zhang, J.T., Zhu, J.Q., Zhu, Q., Liu, H., Gao, X.S. and Zhang, H.X. (2009) Fatty acid desaturase-6 (Fad6) is required for salt tolerance in *Arabidopsis thaliana*. *Biochem. Biophys. Res. Commun.* 390: 469–474.